# Localizing scatterers from surf noise cross correlations

**Jie Li,[1,a] Peter Gerstoft,[2] Dazhi Gao,[1] Guofu Li,[1] and Ning Wang[1]**
[1]*College of Information Science and Engineering, Ocean University of China, Qingdao 266100, China*
[2]*Scripps Institution of Oceanography, University of California San Diego, La Jolla, California 92093-0238, USA*
*jil004@ucsd.edu, gerstoft@ucsd.edu, dzgao@ouc.edu.cn, zhenglimuyun@sina.com, wangyu@public.qd.sd.cn*

**Abstract:** The backscattered travel-time structure is obtained by cross-correlating air-acoustic ocean surf noise recorded on microphone pairs (separation ~2 m) on the beach. The scatterer is a 20 cm radius Polyvinyl chloride pipe 2.5 m landside of the microphone array. Arrivals corresponding to the time-difference (travel-time difference between two scatterer-receiver paths) and scattered (travel time for receiver-scatterer-receiver path) waves emerge in the cross-correlation functions in a backscattering configuration. Theoretically, only a microphone pair is needed to locate the scatterer using the time-difference and scattered travel times. Localization of the scatterer is demonstrated with the microphone array on the beach.


[CCC]
**Date Received:** September 6, 2016 **Date Accepted:** November 9, 2016

## 1. Introduction

Forming acoustic images using ambient noise as the sole illumination is a passive imaging method to observe silent objects. Passive imaging with ambient noise is classified into incoherent and coherent, depending on whether intensity or phase information is employed. Buckingham *et al.* (1992) demonstrated that the ambient noise field provides a form of "acoustic daylight" beneath the sea surface. They designed the acoustic daylight ocean noise imaging system and observed targets 38 m away incoherently (Buckingham *et al.*, 1996). However, coherent passive imaging is mainly based on Green's function retrieval. The Green's function between two receivers is obtained by cross-correlating diffuse noise field recorded on these receivers (Lobkis and Weaver, 2001). Based on this idea, Garnier and Papanicolaou (2009) located in simulation a point scatterer 50 m away. Lani *et al.* (2011) employed a capacitive micro machined ultrasonic transducer array immersed in water to image a point scatterer in oil 1.3 mm above the array using thermal mechanical noise. Davy *et al.* (2013) localized a 5-cm diameter aluminum cylinder with ambient thermal radiations in anechoic and reverberant cavities.

We introduce a coherent passive localization technique based on time-difference waves and scattered waves in an acoustic daylight configuration, where the sensors receive backscattered waves, thus a backscattering configuration. In theory it involves only two sensors, and uses both scattered and time-difference waves, while other methods use these waves somewhat separately. We demonstrate this method with an outdoor experiment using surf noise.

## 2. Localization of scatterer in a backscattering configuration

Snieder *et al.* (2008) retrieved the two-point Green's function in presence of a scatterer for uniformly distributed sources in a three-dimensional wave propagation configuration. The theory is summarized based on their idea but generalized for nonuniformly distributed sources, and is further applied to a backscattering configuration with a line source.

We assume point sources $q(\mathbf{r})$ distributed on a far-field sphere surface with a single scatterer C at its origin, see Fig. 1(a). The scattering amplitude is $f(\hat{\mathbf{n}}, \hat{\mathbf{n}}')$, where $\hat{\mathbf{n}}'$ and $\hat{\mathbf{n}}$ are the directions of incoming and scattered waves, respectively. The sound

[a]Author to whom correspondence should be addressed. Also at: Scripps Institution of Oceanography, University of California San Diego, La Jolla, CA 92093-0238, USA.

 

pressure from the point source $\mathbf{r}$ to receiver $\mathbf{r}_A$ in the $x$-$z$ plane, is the sum of direct and scattered wavefields in the frequency domain

$$p(\mathbf{r}_A,\mathbf{r}) = q(\mathbf{r})G_0(\mathbf{r}_A,\mathbf{r}) + q(\mathbf{r})G_s(\mathbf{r}_A,\mathbf{r}). \tag{1}$$

Assuming $\mathbf{r}$ and $\mathbf{r}_A$ are far from the scatterer, we have

$$G_0(\mathbf{r}_A,\mathbf{r}) = -\frac{\exp(ik|\mathbf{r}-\mathbf{r}_A|)}{4\pi|\mathbf{r}-\mathbf{r}_A|},$$
$$G_S(\mathbf{r}_A,\mathbf{r}) = -\frac{\exp(ikr)}{4\pi r} f(\hat{\mathbf{r}}_A,-\hat{\mathbf{r}})\frac{\exp(ikr_A)}{r_A}, \tag{2}$$

where $k$ is the wavenumber, $r = \|\mathbf{r}\|$, $r_A = \|\mathbf{r}_A\|$. For uncorrelated noises, $\langle q(\mathbf{r})q^*(\mathbf{r}')\rangle = Q(\mathbf{r})\delta(\mathbf{r}-\mathbf{r}')$, where $\langle\cdot\rangle$ denotes the ensemble averaging, $Q(\mathbf{r})$ the noise power spectral density, and $\delta$ the Dirac delta function.

By cross-correlating noise wavefields, Eq. (1), at $\mathbf{r}_A$ and $\mathbf{r}_B$, and integrating over source location $\mathbf{r}$ using the stationary phase approximation, we have (Snieder *et al.*, 2008)

$$\oint p(\mathbf{r}_A,\mathbf{r})p^*(\mathbf{r}_B,\mathbf{r})dS = \frac{i}{2k}\left[Q_{1\alpha}G_0(\mathbf{r}_A,\mathbf{r}_B) - Q_{1\beta}G_0^*(\mathbf{r}_A,\mathbf{r}_B) + Q_{2\alpha}G_S(\mathbf{r}_A,\mathbf{r}_B) - Q_{3\alpha}G_S^*(\mathbf{r}_A,\mathbf{r}_B)\right]$$
$$+\frac{\exp\left(ik(r_A-r_B)\right)}{8\pi k r_A r_B}\left[iQ_{2\beta}f(\hat{\mathbf{r}}_A,\hat{\mathbf{r}}_B) - iQ_{3\beta}f^*(\hat{\mathbf{r}}_A,\hat{\mathbf{r}}_B)\right.$$
$$\left.+\frac{k}{2\pi}\oint f(\hat{\mathbf{r}}_A,\hat{\mathbf{r}})f^*(\hat{\mathbf{r}}_B,\hat{\mathbf{r}})d\Omega\right], \tag{3}$$

where the surface integral is related to the solid angle, $dS = r^2 d\Omega$. Five waves are retrieved: causal and anti-causal direct waves, $G_0$ and $G_0^*$, with source power from stationary points $Q_{1\alpha}$ and $Q_{1\beta}$ (travel times $\|\mathbf{r_A}-\mathbf{r_B}\|/c$ and $-\|\mathbf{r_A}-\mathbf{r_B}\|/c$), causal and anti-causal scattered waves, $G_S$ and $G_S^*$, with stationary points $Q_{2\alpha}$ and $Q_{3\alpha}$ [travel times $(r_A+r_B)/c$ and $-(r_A+r_B)/c$], and a time-difference wave from $Q_{2\beta}$, $Q_{3\beta}$ and an integration term [travel-time $(r_A-r_B)/c$], see Fig. 1(b). Physically, no wave is arriving at the time difference $(r_A-r_B)/c$, they are spurious arrivals (Snieder *et al.*, 2006; Brooks and Gerstoft, 2007). For uniformly distributed sources, $Q(\mathbf{r})$ is constant and is neglected. This simplifies Eq. (3) (Snieder *et al.*, 2008),

$$\oint p(\mathbf{r}_A,\mathbf{r})p^*(\mathbf{r}_B,\mathbf{r})dS = -\frac{1}{k}\mathrm{Im}G(\mathbf{r}_A,\mathbf{r}_B) + \frac{\exp\left(ik(r_A-r_B)\right)}{4\pi k r_A r_B}$$
$$\times\left[-\mathrm{Im}(f(\hat{\mathbf{r}}_A,\hat{\mathbf{r}}_B)) + \frac{k}{4\pi}\oint f(\hat{\mathbf{r}}_A,\hat{\mathbf{r}})f^*(\hat{\mathbf{r}}_B,\hat{\mathbf{r}})d\Omega\right], \tag{4}$$

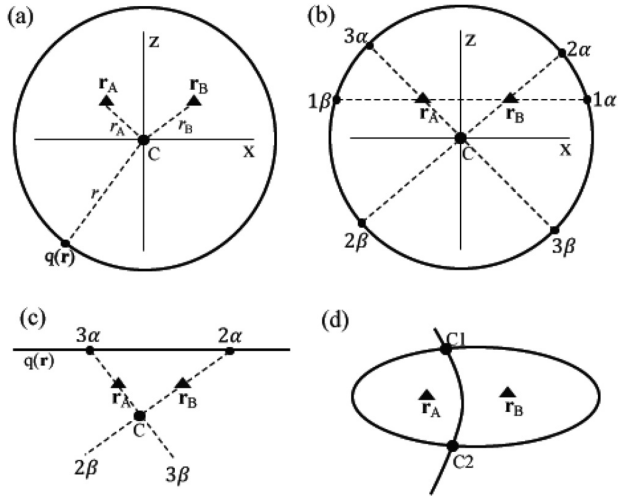


Fig. 1. (a) Definition of geometric variables. (b) Stationary points of direct, scattered, and time-difference waves. (c) A backscattering configuration, receiver pair $\mathbf{r_A}$ and $\mathbf{r_B}$ is located between line source and scatterer C. The stationary points of scattered waves ($2\alpha$, $3\alpha$) and time-difference waves ($2\beta$, $3\beta$), are shown. (d) From the travel times of scattered and time-difference waves, the scatterer is positioned at intersections (C1, C2) of an ellipse and one branch of a hyperbola.

where $G = G_0 + G_S$ is the sum of direct and scattered waves. According to the generalized optical theorem (Newton, 1976), the square bracket term is zero, and thus there is no time-difference wave. The time-difference waves are mostly treated as disturbances in the applications, and suppressed (Wapenaar, 2006; King and Curtis, 2012). However, these waves contain information about the scatterers, and used in ultrasonics to locate scatterers actively (Harmankaya *et al.*, 2013).

We introduce a localization method based on both scattered and time-difference waves in a backscattering configuration [Fig. 1(c)]. For an uncorrelated and uniformly distributed line source q(**r**), there exists five waves, see Eq. (3). Sources from points $2\alpha$ and $3\alpha$ [Fig. 1(c)] contribute to the causal and anti-causal scattered waves, respectively. There are no sources at $2\beta$ and $3\beta$ [Fig. 1(c)], thus $Q_{2\beta} = 0$, $Q_{3\beta} = 0$. The last integration term in Eq. (3) is not zero when integrated over a line source. Therefore, the last square bracket term in Eq. (3) cannot be simplified as the generalized optical theorem, and the time-difference wave emerges. Let the travel time from the scatterer (C) to the two receivers be $r_{AC}/c$ and $r_{BC}/c$, thus the travel times of causal scattered wave and time-difference wave are $t_{SC} = (r_{AC} + r_{BC})/c$ and $t_{\text{diff}} = (r_{AC} - r_{BC})/c$. These equations form an ellipse and one branch of a hyperbola from which the scatterer is localized at points C1 and C2 [Fig. 1(d)]. As the scatterer is in a backscattering configuration, only location C2 satisfies this condition.

### 3. Data processing procedure and experimental results

Broadband ambient noise was recorded at 20 kHz sampling frequency for 40 min using 14 microphones at Shilaoren Beach, Qingdao, China from 04:43 UTC April 25, 2015. Ambient noises are mainly generated by ocean surf noise. From Figs. 2(a) and 2(b), the experiment configuration is a backscattering configuration. Microphones M1–M11 are positioned at a stand parallel to the coastline with spacing 8 cm, M12–M14 are each at the top of a tripod. All the microphones are at 1 m height and wrapped by a sponge to attenuate wind noise. The cylinder is a hollow Polyvinyl chloride (PVC) pipe (radius 20 cm, height 2 m), standing 2.5 m from the microphone array. The recording system consists of 14 microphones (MNP20, SKC, Beijing, China), a 16-channel amplifier (Custom-made, SKC, Beijing, China), and a signal recorder (PXI 1042Q, National Instruments, Austin, TX).

Figure 2(c) displays the spectrogram of the acoustic data. Ocean waves with 10 s period is seen. Conventional plane wave beamforming with Kaiser spatial shading is performed [Fig. 2(d)]. We define the direction of 0° orthogonal to the array, while the direction of 90° parallel to the array and from M1 to M11. Noise sources below 400 Hz are difficult to distinguish (at 400 Hz, array aperture is about $\lambda$). For higher frequencies, noise sources mainly focus on [−40°, 40°], with the highest peak at 4°.

In this backscattering configuration, we care about the scattering intensity in the backward (seaside) direction. From Morse and Ingard [1968, Eq. (8.1.3)], the backward scattered intensity grows sharply for $ka < 1$, and nearly constant $ka > 1$ despite some initial oscillations [see Fig. 3(a)]. The main frequency band is 0–4 kHz, see Fig. 2(c), thus $ka$ ranges from 0 to 14.8 ($a = 0.2$ m). As predicted by Fig. 2(d), higher frequencies attenuate faster, and focus on a narrow angle band. For these three reasons, the cross correlation function (CCF) frequency band is 270 to 3000 Hz, where $ka$ ranges from 1 to 11. The snapshot size for cross-correlation processing in the time domain is $T\text{snap} = 1$ s, and total averaging time is $T\text{ave} = 3$ min. The scattered and time-difference waves begin to converge when $T\text{ave} = 40$ s, see Fig. 3(b).

Figure 4(a) shows all the CCFs from 91 microphone pairs arranged by separation. The bottom CCFs (separation from 0.08 to 1.15 m, marked by label "B") come from the 66 pairs between M1 and M12. The middle CCFs (separation 1.3 to 2.2 m, label "M") are from 12 pairs between M1 and M12 and M13. The top 13 CCFs (separation 1.9 to 3.6 m, label "T") are from 13 pairs between M1 and M13 and M14.

Given the distribution of surf noise energy along the coast [Fig. 2(d)] and orientation of microphone pairs, the maxima of direct waves might not be time symmetrical (Sabra *et al.*, 2005). For the scattered waves, $Q_{2\alpha}$ and $Q_{3\alpha}$ is the same, but the distance from $2\alpha$ and $3\alpha$ to the microphones are different, thus geometric attenuation is different [Fig. 1(c)]. This causes the maxima of causal and anti-causal scattered waves to not be symmetrical for some pairs. For example, the amplitudes of anti-causal scattered waves are higher than the causal scattered waves for the middle and top part (separation > 1.3 m), while almost equal for the first 66 pairs (separation < 1.3 m). High-peaks and suppressed peaks between direct waves denoted by arrows are caused

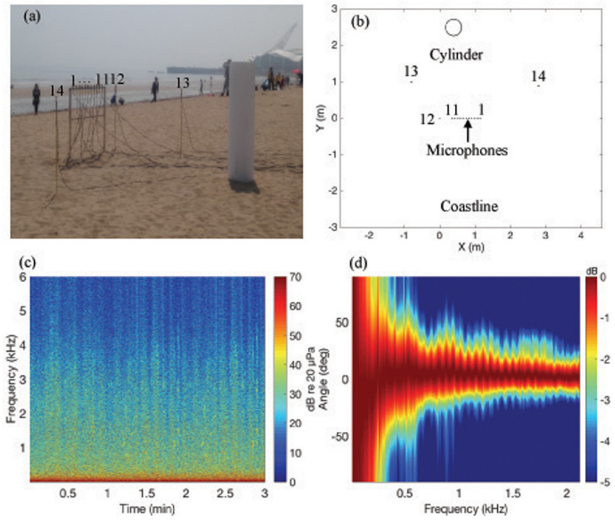


Fig. 2. (Color online) (a) Layout of field experiment. The numerals 1–14 indicate positions of 14 microphones. (b) Schematic diagram of (a). (c) Spectrogram of the noise recorded on M1. (d) Conventional plane wave beamforming result from microphone array M1–M11.

by strong surf noise at 4° [Fig. 2(d)]. For the first 66 pairs, these high-peaks overlap with time-difference waves, so it is difficult to retrieve these time-difference waves. For the 25 pairs with separation $> 1.3$ m, the high-peaks and the time-difference waves are separated in the time domain, we can suppress these high-peaks. Among 25 CCFs, 22 CCFs show clear scattered and time-difference waves, which come from microphone pairs M1–M11 and M13 (separation 1.5–2.2 m), and M1–M11 and M14 (separation 1.9–2.6 m). Time-difference waves from microphone pairs M12–M13 (separation 1.3 m) and M12–M14 (separation 2.9 m), and scattered waves from microphone pair M13–M14 (separation 3.6 m) are not obvious. Thus these pairs are not used.

In theory, only one microphone pair is needed to obtain the location of scatterer (see Sec. 2), however, when there exists directional noise, we may need an array or longer averaging time to localize it. In Fig. 4(b) we illustrate the passive localization results from 22 CCFs stated above to make the result more convincing, and also show the possibility of imaging the boundary of cylinder with more microphone pairs. The assumed sound speed is $c = 340$ m/s. Each pair gives one estimated location (+) around the seaside boundary of cylinder, due to microphone pairs having different scattering points on the PVC pipe. The estimated locations clustered around coordinate (0.2, 2.3) are from microphone pairs M1–M11 and M13, and locations clustered at coordinate (0.5, 2.4) are from microphone pairs M1–M11 and M14.

We have focused on a backscattering configuration. Other configurations may not work, e.g., the forward scattering configuration with scatterer between line source and sensors. Only the time-difference wave is retrieved, thus the cylinder cannot be located by one single pair of sensors.

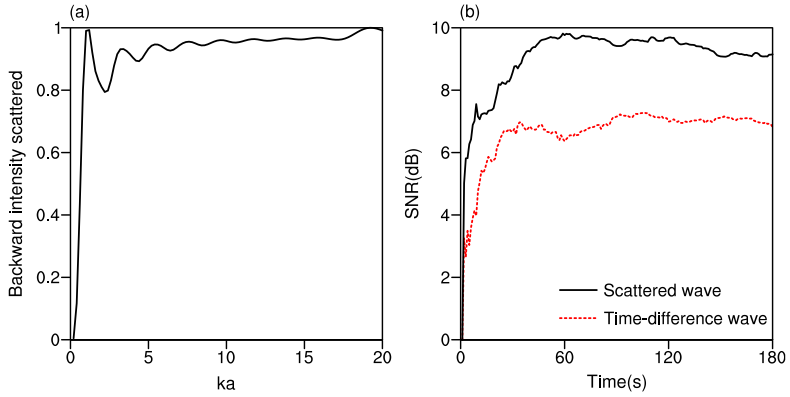


Fig. 3. (Color online) (a) Total backscattered strength. (b) SNR of scattered and time-difference waves with averaging time.

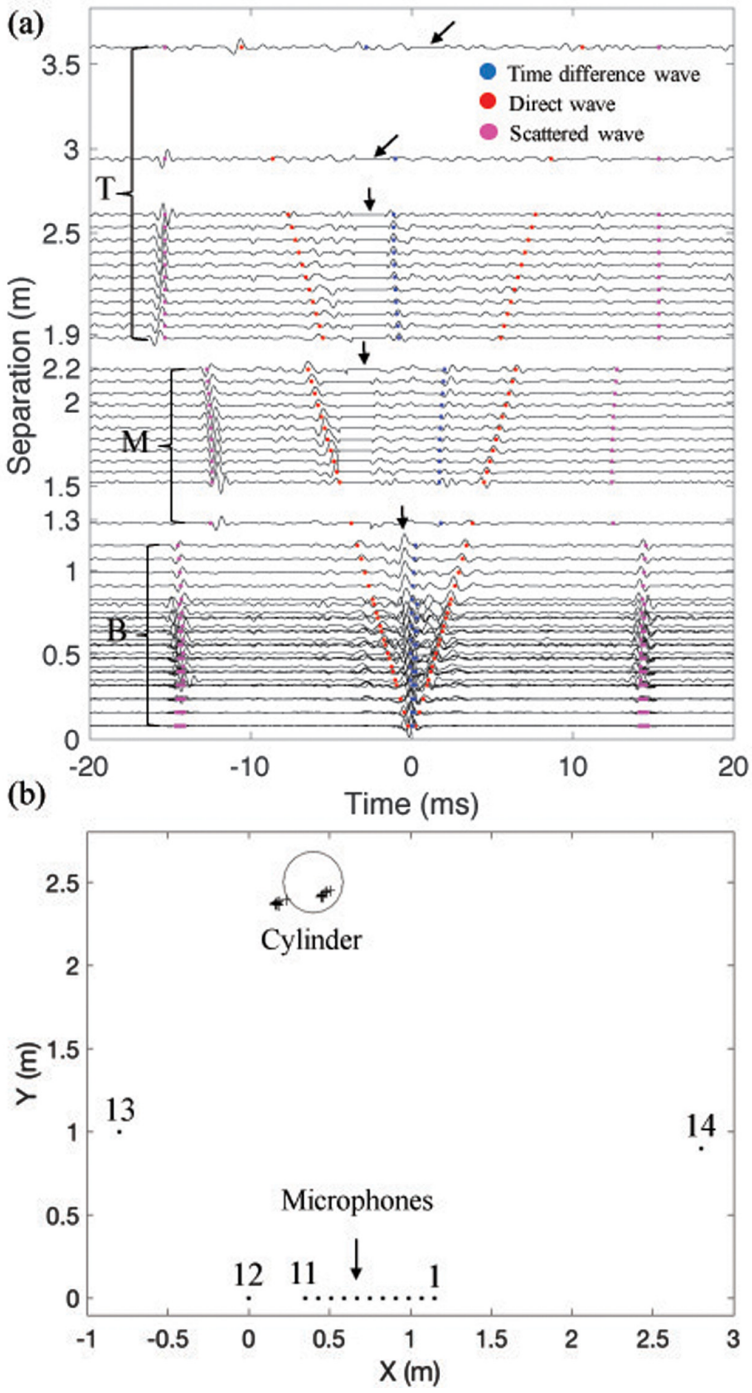


Fig. 4. (Color online) (a) The CCFs of 91 microphone pairs over 3 min. The CCFs are normalized, and the theoretical arrival time of direct, time-difference, and scattered waves are marked by dots. High-peaks and suppressed peaks marked by arrows are caused by surf noise at 4°. (b) Passive localization from 22 CCFs [most CCFs marked M and T in (a)]. The location of PVC cylinder (circle) and estimated location of each pair (+) are shown.

## 4. Conclusion

When performing noise cross correlation in a backscattering configuration, time-difference waves are present due to strict requirements for the full recovery of the Green's function. These waves can be employed to retrieve information of the environment. We retrieve the travel times of scattered and time-difference waves for a PVC cylinder scatterer in the acoustic backscattering configuration. By combining these two arrivals, we localize the cylinder with two microphones. With more microphones, the shape of the scatterer illuminated by noise sources might be obtained.

## Acknowledgments

This work was supported by the National Natural Science Foundation of China (Grant Nos. 11374270 and 11374271), the China Scholarship Council (Grant No. 201506330018), and the Office of Naval Research (Grant No. N00014-11-1-0439).

## References and links

Brooks, L. A., and Gerstoft, P. (**2007**). "Ocean acoustic interferometry," J. Acoust. Soc. Am. **121**, 3377–3385.

Buckingham, M. J., Berkhout, B. V., and Glegg, S. A. L. (**1992**). "Imaging the ocean with ambient noise," Nature **356**, 327–329.

Buckingham, M. J., Potter, J. R., and Epifanio, C. L. (**1996**). "Seeing underwater with background noise," Sci. Am. **274**, 86–90.

Davy, M., Fink, M., and Rosny, J. D. (**2013**). "Green's function retrieval and passive imaging-from correlations of wideband thermal radiations," Phys. Rev. Lett. **110**, 203901.

Garnier, J., and Papanicolaou, G. (**2009**). "Passive sensor imaging using cross correlations of noisy signals in a scattering medium," J. Imaging. Sci. **2**, 396–437.

Harmankaya, U., Kaslilar, A., Thorbecke, J., Wapenaar, K., and Draganov, D. (**2013**). "Locating near-surface scatterers using non-physical scattered waves resulting from seismic interferometry," J. Appl. Geophys. **91**, 66–81.

King, S., and Curtis, A. (**2012**). "Suppressing nonphysical reflections in Green's function estimates using source-receiver interferometry," Geophysics. **77**, Q15–Q25.

Lani, S., Satir, S., Gurun, G., Sabra, K. G., and Degertekin, F. L. (**2011**). "High frequency ultrasonic imaging using thermal mechanical noise recorded on capacitive micromachined transducer arrays," Appl. Phys. Lett. **99**, 224103.

Lobkis, O. I., and Weaver, R. L. (**2001**). "On the emergence of the Green's function in the correlations of a diffuse field," J. Acoust. Soc. Am. **110**, 3011–3017.

Morse, P. M., and Ingard, K. U. (**1968**). *Theoretical Acoustics* (Princeton University Press, Princeton, NJ), 402 pp.

Newton, R. G. (**1976**). "Optical theorem and beyond," Am. J. Phys. **44**, 639–642.

Sabra, K. G., Gerstoft, P., Roux, P., Kuperman, W. A., and Fehler, M. C. (**2005**). "Extracting time-domain Green's function estimates from ambient seismic noise," Geophys. Res. Lett. **32**, L03310, doi:10.1029/2004GL021862.

Snieder, R., van Wijk, K., and Haney, M. (**2008**). "The cancellation of spurious arrivals in Green's function extraction and the generalized optical theorem," Phys. Rev. E. **78**, 036606.

Snieder, R., Wapenaar, K., and Larner, K. (**2006**). "Spurious multiples in seismic interferometry of primaries," Geophysics **71**, SI111–SI124.

Wapenaar, K. (**2006**). "Green's function retrieval by cross-correlation in case of one-sided illumination," Geophys. Res. Lett. **33**, L19304, doi:10.1029/2006GL027747.